Experimental Characterization of the MIMO Wireless Channel

Jon W. Wallace* and Michael A. Jensen
Department of Electrical and Computer Engineering
Brigham Young University
459 CB, Provo, UT 84602
wallacej@et.byu.edu, jensen@ee.byu.edu

I. Introduction The increasing demand for capacity in wireless systems has motivated considerable research aimed at achieving higher throughput on a given bandwidth. One important recent discovery shows that in a multipath environment, the use of space-time coding with multiple antennas on both ends of the link can increase the capacity of the wireless channel [1]–[3]. Assessing the performance of these algorithms requires an improved understanding of the complex spatial behavior of wireless multiple input multiple output (MIMO) channels [4].

In this work, we report the development of an experimental platform designed to measure the transfer matrix for indoor and outdoor MIMO channels. The key aspects of the hardware system are presented, including a discussion of measurement issues and data processing approaches. Representative data obtained with the instrument in several indoor environments are presented. These results reveal the large increase in capacity that can be achieved using MIMO architectures coupled with space-time coding implementations.

II. Measurement System The goal of this effort is to directly measure the wireless MIMO channel transfer matrix $\mathbf{H}$, where the element $H_{mn}(\omega)$ represents the frequency dependent transfer function between the n^{th} transmitter and m^{th} receiver antennas. The experimental platform, depicted in Figure 1, uses a custom MIMO communications system operating between 0.8 and 6 GHz. The transmitter, shown in Figure 2, uses a digital pattern generator (DPG) to create N unique binary (± 1) codes. These codes are fed into the custom RF chassis shown in Figure 3 where they are mixed with a local oscillator (LO) to produce N distinct co-channel binary phase shift keyed (BPSK) signals. The resulting signals are amplified to 0.5 W and fed into one of the N transmit antennas.

The receiver uses a custom RF chassis to amplify and downconvert the signals from each of the M antennas. The resulting M intermediate frequency (IF) signals are low-pass filtered, amplified, and sampled using a 16-channel 1.25 Msample/s A/D card for storage on the PC. Two different antenna arrays have been constructed for the experiments. The first design is a 4-element dual-polarization patch array with half-wavelength element spacing. The second consists of a square metal plate with a two-dimensional grid of 33×33 holes spaced at roughly 1.5 cm intervals. Monopole antennas are placed in the holes to achieve a wide variety of array geometries.

III. Data Processing The raw data collected using the measurement platform is processed to obtain estimates of the time-variant channel matrix. The technique consists of 3 basic steps: (1) code search, (2) carrier recovery, and (3) channel estimation.

Code Search The first step in the data post-processing is to determine the alignment of the modulating codes. As shown in Figure 4, the method begins by correlating the signal from one of the M receive Antennas with a baseband representation of one of the transmit codes. An FFT of this result produces a peak at the IF when the known code and the code in the receive signal are aligned. This search process may be expedited by (1) using a shortened code and (2) adaptively reducing the step size as the search progresses. Additionally, if the signal carrying the specified code is weak, the maximum correlation may not occur at codeword alignment. To overcome this, our procedure searches over every combination of receive channel and codeword to ensure accurate code synchronization.

Carrier Recovery A rough estimate of the intermediate frequency is obtained from the peak of the FFT taken during the code search process. This frequency is then refined using a subplex optimization loop that maximizes the magnitude of the Discrete Time Fourier Transform (DTFT) of the despread signal (known aligned code multiplied by the receive signal). Following estimation of the frequency, the time evolution of the phase is recovered using the procedure in Figure 5. In this method, a recovery window is shifted along the despread receive signal at one sample increments. At each position, the signal is correlated against a complex sinusoid at the estimated IF frequency. The estimated phase at the center of the window is the angle of the complex result of the correlation. This phase estimate is finally smoothed by an averaging window.

0-7803-7070-8/01/$10.00 ©2001 IEEE

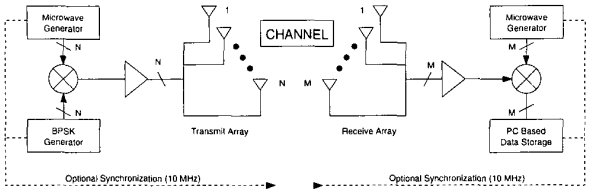

Figure 1: High level system diagram of the narrowband wireless MIMO measurement system

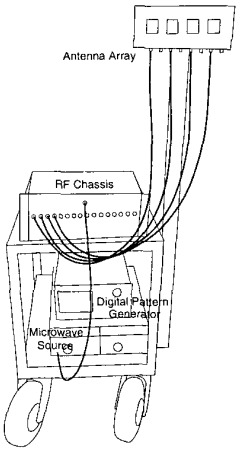

Figure 2: Transmit system diagram.

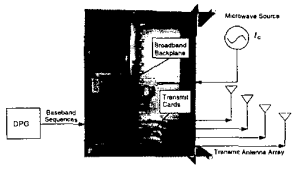

Figure 3: Custom RF chassis for the transmit subsystem.

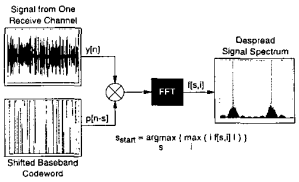

Figure 4: Basic method for finding codeword start sample when exact carrier frequency is unknown.

Channel Estimation The IF signal on the m^{th} receive channel is composed of N BPSK codes, with each code possessing an amplitude A_{mn} and phase ϕ_{mn}. If $p_n[k]$ represents the k^{th} sample of the n^{th} code, the discrete received signal is given as

$$y_m[k] = \sum_{n=0}^{N-1} A_{mn}\, p_n[k]\, \cos(\Omega_1 k + \phi_k + \phi_{mn}) \tag{1}$$

where Ω_1 is the discrete carrier frequency and ϕ_k is the randomly varying carrier phase. Note that for simplicity in deriving the inverse relationship, additive noise has been ignored.

To construct channel matrices, we must infer the channel parameters A_{mn} and ϕ_{mn} from the received sequence $y_m[k]$. To obtain a maximum likelihood estimation of these values, we multiply $y_m[k]$ by the i^{th} code and the complex signal $c[k] = e^{-j(\Omega_1 k + \phi_k)}$ and subsequently average over $K = (k_2 - k_1 + 1)$ samples to produce

$$R_{mi} = \frac{1}{2K} \sum_{k=k_1}^{k_2} \sum_{n=0}^{N-1} \left[\widetilde{A}_{mn} + \widetilde{A}^*_{mn} e^{-j2(\Omega_1 k + \phi_k)} \right] p_{ni}[k] \tag{2}$$

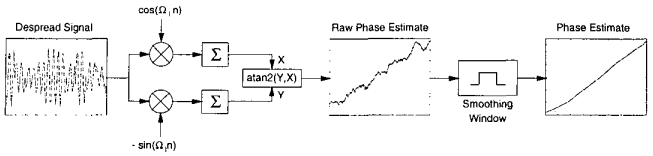

Figure 5: Carrier phase recovery method

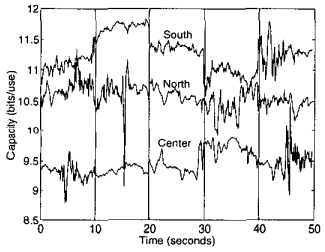

Figure 6: Capacity as a function of time at three locations in a large student computer lab. Vertical lines show a 20 second pause between measurements at a single location.

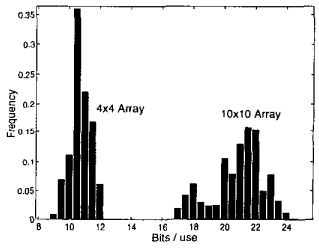

Figure 7: Histogram of capacity over all times and locations.

where $p_{ni}[k] = p_n[k]p_i[k]$ and $\widetilde{A}_{mn} = A_{mn}e^{j\phi_{mn}}$. Dividing the equation into real and imaginary parts produces the relations

$$R_{R,mi} = \frac{1}{2K}\sum_{k=k_1}^{k_2}\sum_{n=0}^{N-1}[A_{R,mn}(1+\alpha_k) - A_{I,mn}\beta_k]\,p_{ni}[k]$$

$$R_{I,mi} = \frac{1}{2K}\sum_{k=k_1}^{k_2}\sum_{n=0}^{N-1}[A_{I,mn}(1-\alpha_k) - A_{R,mn}\beta_k]\,p_{ni}[k] \qquad (3)$$

where $\alpha_k = \cos[2(\Omega_1 k + \phi_k)]$ and $\beta_k = \sin[2(\Omega_1 k + \phi_k)]$. These equations can now be formed into a block matrix equation and solved for the elements $\widetilde{A}_{mn} = A_{R,mn} + jA_{I,mn} = H_{mn}$.

Error in the channel matrix estimates may arise from a number of sources: additive receiver noise, carrier recovery error, quantization, non-ideal system impulse response, transmitter crosstalk, and receiver crosstalk. The effect of these error sources in isolation can be found analytically, and the net effect from all contributions may be obtained through simulations. Much of this error is removed from the system using a calibration procedure, with correction coefficients applied during data processing.

Representative Results Some preliminary measurements have been taken with the experimental platform discussed. For these trials, the receiver was placed in a large student computer lab and data was collected at 12 locations moving from the north to south side spaced by about 2 m. The carrier frequency was 2.45 GHz with a BPSK code rate of 12.5 kb/s. The transmitter was placed in a smaller room adjacent to the computer lab. Both the 4-element patch array and a 10-element linear array of monopoles were used for data collection. Figure 6 plots the capacity at the north side, center, and south side of the lab as a function of time. Here, the water-filling solution was used with an assumed average SISO SNR of 10-dB (see [5]). Jumps in the capacity are a result of intervals where no data is being collected. Figure 7 shows a histogram of capacity across all probing times and locations. Finally, Figure 8 shows the transmit and

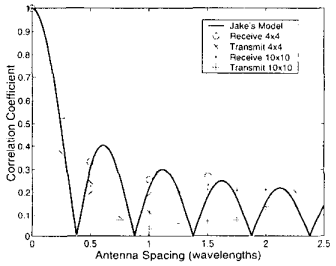

Figure 8: Magnitude of the correlation coefficient for transmit and receive antennas compared with Jake's model.

receive correlations for this test site compared with Jake's model [6]. Receive correlation is found by computing the correlation coefficient of signals on receive antennas separated by a given spacing, over all probe times, locations, and transmit antennas. Transmit correlation is found similarly, by exchanging roles of transmit and receive.

IV. Conclusion

Wireless communication systems employing multiple transmit and receive antennas have potentially greater capacity than their single antenna counterparts on the same bandwidth. Understanding the gains that are possible with such systems requires detailed knowledge of the MIMO channel transfer matrix. This paper has presented a system capable of measuring wireless MIMO channel response over the 0.8 to 6 GHz frequency range with up to 16 transmitters and receivers. Details of the required hardware and data processing were outlined along with representative data. Data collected by this platform will aid in the assessment of the validity of analytical and numerical channel models. Also, the data may provide a starting point for new models which capture the complex spatial behavior of indoor and outdoor multipath environments.

Acknowledgements: This work was supported by the National Science Foundation under Wireless Initiative Grant CCR 99-79452.

References

[1] G. J. Foschini and M. J. Gans, "On limits of wireless communications in a fading environment when using multiple antennas", *Wireless Personal Communications*, vol. 6, no. 3, pp. 311–335, March 1998.

[2] T. L. Marzetta and B. M. Hochwald, "Capacity of a mobile multiple-antenna communication link in Rayleigh flat fading", *IEEE Trans. Information Theory*, vol. 45, no. 1, pp. 139–157, May 1999.

[3] G. Golden, C Foschini, R Valenzuela, and P. Wolniansky, "Detection algorithm and initial laboratory results using V -BLAST space-time communication architecture", *Electronic Letters*, vol. 35, no. 1, pp. 14–15, Jan. 1999.

[4] Q. Spencer, B. Jeffs, M. Jensen, and A. Swindlehurst, "Modeling the statistical time and angle of arrival characteristics of an indoor multipath channel", *IEEE J. Selected Areas Commun.*, vol. 18, no. 3, pp. 347–360, Mar. 2000.

[5] G. G. Rayleigh and J. M. Cioffi, "Spatio-temporal coding for wireless communication", *IEEE Transactions on Communications*, vol. 46, no. 3, pp. 357–366, March 1998.

[6] W. C. Jakes, *Microwave Mobile Communications*, IEEE Press, 1993.